Enhancing cell penetration and proliferation in chitosan hydrogels for tissue engineering applications

Chengdong Ji[a], Ali Khademhosseini[b,c,d], Fariba Dehghani[a,*]

[a] School of Chemical and Biomolecular Engineering, University of Sydney, Sydney 2006, Australia
[b] Center for Biomedical Engineering, Department of Medicine, Brigham and Women's Hospital, Harvard Medical School, Boston, MA 02139, USA
[c] Harvard-MIT Division of Health Sciences and Technology, Massachusetts Institute of Technology, Cambridge, MA 02139, USA
[d] Wyss Institute for Biological Inspired Engineering at Harvard University, Boston, MA 02115, USA

ARTICLE INFO

ABSTRACT

The aim of this study was to develop a process to create highly porous three-dimensional (3D) chitosan hydrogels suitable for tissue engineering applications. Chitosan was crosslinked by glutaraldehyde (0.5 vol %) under high pressure CO_2 at 60 bar and 4 °C for a period of 90 min. A gradient-depressurisation strategy was developed, which was efficient in increasing pore size and the overall porosity of resultant hydrogels. The average pore diameter increased two fold (59 μm) compared with the sample that was depressurised after complete crosslinking and hydrogel formation (32 μm). It was feasible to achieve a pore diameter of 140 μm and the porosity of hydrogels to 87% by addition of *Acacia gum* (AG) as a surfactant to the media. The enhancement in porosity resulted in an increased swelling ratio and decreased mechanical strength. On hydrogels with large pores (>90 μm) and high porosities (>85%), fibroblasts were able to penetrate up to 400 μm into the hydrogels with reasonable viabilities (∼80%) upon static seeding. MTS assays showed that fibroblasts proliferated over 14 days. Furthermore, aligned microchannels were produced within porous hydrogels to further promote cell proliferation. The developed process can be easily used to generate homogenous pores of controlled sizes in 3D chitosan hydrogels and may be of use for a broad range of tissue engineering applications.

Crown Copyright © 2011 Published by Elsevier Ltd. All rights reserved.

1. Introduction

Porosity plays a significant role in the overall function of tissue engineering scaffolds [1–3]. In particular, pore characteristics such as pore size and interconnectivity are critical in hydrogel properties such as swelling, mechanical strength and cell adhesion [1]. Enhancing porosity and pore interconnectivity have been shown to enhance nutrient diffusion and waste exchange [4], while decreasing the mechanical properties of hydrogels [5]. Upon implantation, porosity allows for local angiogenesis that is essential for vascularisation [1].

Various methods such as freeze-drying, salt leaching and gas foaming have been used to produce porous hydrogel scaffolds with controlled pore size and interconnectivity [1]. In the freeze-drying process the pore size and overall porosity can be controlled by freezing temperature and polymer solution concentration [1,6]. However, the intensive time and energy consumption is undesirable, and the complete dehydration of materials remains a concern

for the inclusion of cells and bioactive molecules during the process [1,2]. In the salt leaching process, salt or sugar particles are used. An advantage of this process is that the pore size can be controlled by using different particle sizes. The drawbacks of this technique are the use of organic solvents and the slow evaporation process (hours-to-days) [1].

High pressure CO_2 has previously been used to produce porosity in hydrogels, such as poly (vinyl alcohol) (PVA) [7], dextran [8], elastin [9,10] and chitosan [11,12]. Cooper and co-workers developed CO_2-water emulsion template technique to fabricate porous PVA hydrogels [7]. This method eliminates the use of organic solvents and can be carried out at moderate conditions (∼25 °C and <120 bar for 12 h). However, a PVA and poly ethylene glycol (PEG) based surfactant (PVA*c*-*b*-PEG-*b*-PVA*c*, M_w = 2000–2000–2000 Da) was used to form stable CO_2-water emulsion, which required extra synthesis and post-removal steps. The pore sizes fabricated in PVA were less than 12 μm, which was undesirable for cell penetration and proliferation in tissue engineering applications [7]. Barbetta and co-workers also used the CO_2 templating technique at 60 °C and 100 bar for 20 h to synthesise a dextran-based porous biomaterial. A polymeric surfactant (per-fluoropolyether, PFPE) was added in the system to form a CO_2-water high internal phase emulsion system [8]. The resulting pore size in

---

this matrix was below 25 μm [8]. While the CO_2 templating technique eliminates the use of organic solvent during pore formation, the issues of lengthy processing time and lack of large pores suitable for cell proliferation still exist.

Previously we fabricated porous hydrogels of elastin and chitosan by using high pressure CO_2 [9–11]. In this method, an aqueous polymer solution with a crosslinker was pressurised by CO_2 to saturate the solution. After crosslinking, the system was depressurised to generate CO_2 bubbles within the crosslinked polymer to fabricate porous hydrogels. This method is faster compared to conventional techniques and eradicates the use of organic solvents [11,13]. The resulting hydrogels had an average pore diameter of 30–40 μm with only a limited numerical fraction (<10%) of large pores (>80 μm). Despite this porosity, fibroblasts were only able to penetrate into the three-dimensional (3D) structure of these hydrogels to a limited depth [11,13].

Microchannels have been created within hydrogel structures to further control and improve porosity and thus diffusion and mass transfer properties [1,14,15]. For example, a rapid micromolding method was developed to fabricate single and dual-channel (400–1600 μm diameter) in agarose. These results demonstrated that larger channels and greater inter-channel distances led to further diffusion of nutrients through the hydrogels [16]. In addition, porous agarose hydrogels with a single microchannel were fabricated by using the sucrose leaching and micromolding technique [17]. The pore diameter (~200 μm) and porosity (0–40%) was controlled by crystal size and concentration of sucrose, respectively. The presence of porosity and the microchannel enhanced the diffusion of biomolecules [17]. These microfludic devices have been used to build cell-laden hydrogel systems [16,17].

The aim of this study was to assess the feasibility of controlling the pore size in chitosan hydrogels by modifying the hydrogel fabrication technique using high pressure CO_2. Chitosan has been widely used in biomedical engineering [12,18]. A gradient-depressurisation step was designed to enhance the pore size and porosity of chitosan hydrogels. *Acacia gum* (AG), a commercialised biopolymer, was used to increase CO_2 bubble formation and subsequently enhance porosity. AG has been approved by the United States Food and Drug Administration (FDA) in the food industry [19]. The effects of operating parameters on pore characteristics, that is, size and porosity were investigated. In turn, the corresponding effects of pore characteristics on hydrogel performances such as swelling ratio, mechanical strength and *in vitro* cell behaviours were

observed. Finally, the microchannel structure was incorporated in the porous chitosan hydrogels, and its effects on cell proliferation were evaluated.

2. Materials and methods

2.1. Materials

Chitosan (medium molecular weight), fluorescein diacetate (FDA), propidium iodide (PI), Dulbecco's modified eagle medium (DMEM), and glutaraldehyde (25 vol %) were purchased from Sigma. MTS [3-(4,5-dimethylthiazol-2-yl)-5-(3-crboxymethoxyphenyl)-2-(4-sulfophenyl)-2H-tetrazolium], Fetal bovine serum (FBS) and penicillin-streptomycin solution (pen-strep) were purchased from Invitrogen. A 0.2 M acetic acid solution was prepared using glacial acetic acid (Ajax Fine Chem) in MilliQ water. Chitosan solution (1.5 wt %) was prepared by dissolving chitosan powder in 0.2 M acetic acid solution. Phosphate buffered saline (PBS, pH 7.2–7.4) was prepared by dissolving PBS tablets (Sigma) in MilliQ water. Tris ((hydroxymethyl)-aminomethane) buffer (0.1 M, pH 7.2–7.4) was prepared by dissolving Tris in PBS; pH was adjusted by adding 1 M HCl. *A. gum* (AG) was supplied from Vic Cherrikoff Food Services Pty Ltd. Food grade CO_2 (99.99%) was supplied from BOC.

2.2. Rheological behaviour of crosslinking chitosan

The rheological behaviour of chitosan crosslinking was measured by using a Rheometer (New Physica MCR 301, Anton Paar). In summary, glutaraldehyde was added into pre-cooled (4 °C) chitosan solution (1.5 wt %) with different weight ratios of AG (0–5 wt %) to commence crosslinking. The volume ratio of glutaraldehyde in chitosan solution used in this study was 0.5 vol %, that is, below the toxic level and adequate for crosslinking [11]. The mixture was stirred using a magnetic stirrer for 1 min and subsequently loaded on a metal sample plate (D-PP25). The system was maintained at 4 °C by using a built-in thermal controller. The storage modulus (G′) and loss modulus (G″), as a function of crosslinking time, were determined from oscillating measurements at a frequency of 1 Hz and strain rate of 1%. Data were recorded by built-in software every 30 s within a total measuring range of 3 h. The gelation point was determined as the time when G′ began to be larger than G″ [20,21].

2.3. Hydrogel fabrication by using a gradient-depressurisation process

The schematic diagram of apparatus used for the porous chitosan hydrogels formation using high pressure CO_2 is shown in Fig. 1. Briefly, chitosan (1.5 wt %) and AG (0–5 wt %) were dissolved in 0.2 M acetic acid solution to form a homogenous mixture, glutaraldehyde was then added into the solution to achieve glutaraldehyde volume ratio of 0.5 vol %, as previously described [11]. The mixture was then injected into a custom made high pressure vessel possessing a frit (50 μm pore size) at the bottom, which prevented solution purging from the vessel. The vessel was sealed and the system was maintained at a constant temperature (4 °C) by submerging the vessel in an ice-water bath. The system was pressurised to a predetermined pressure (60–150 bar) from the bottom of the vessel using a high pressure pump (Model P-50A, Thar Technologies). The system was then isolated and maintained at the
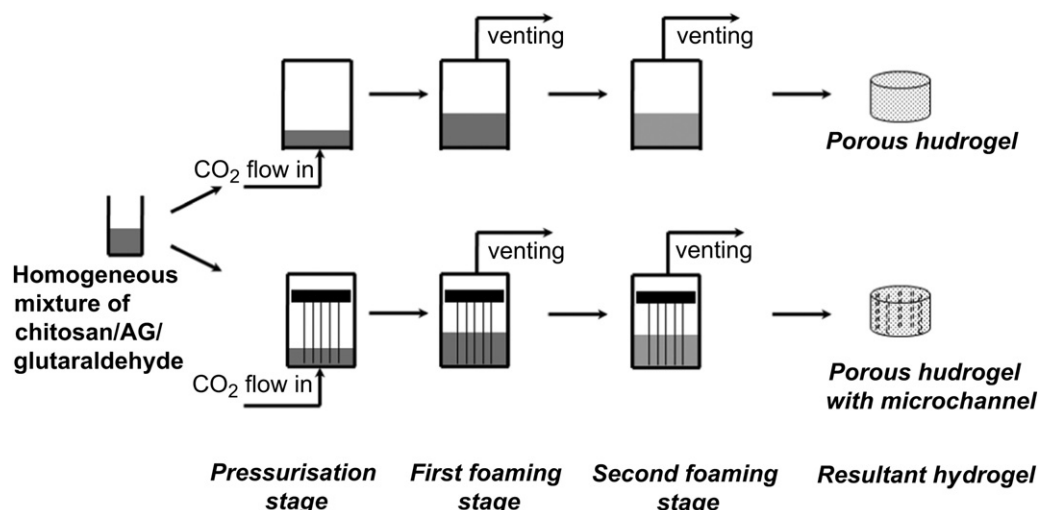
Fig. 1. Schematic diagram of the fabrication steps involved in generating porous chitosan hydrogels without (upper) and with (lower) microchannels.
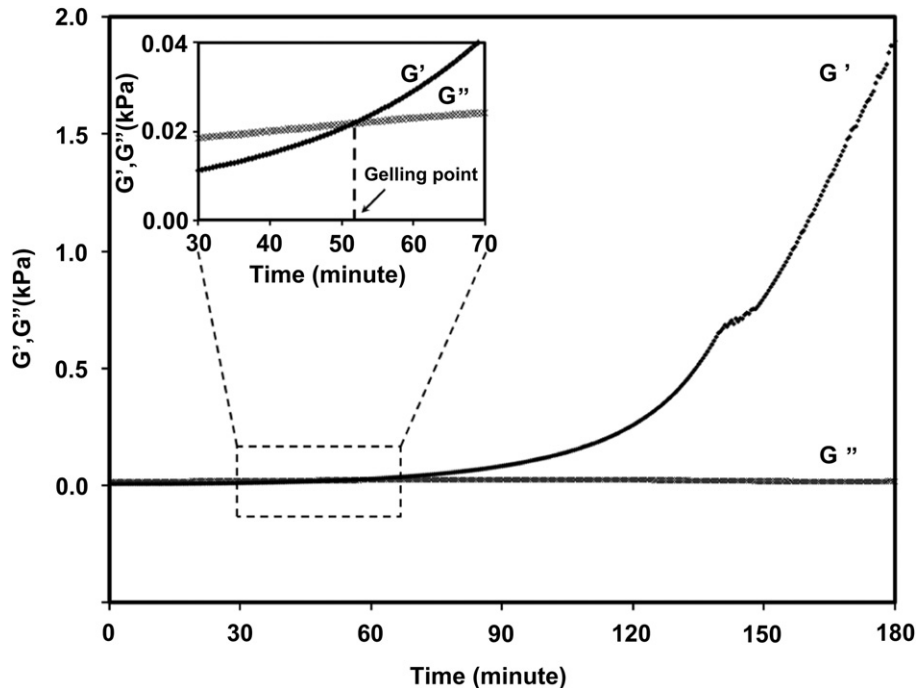
Fig. 2. Rheological behaviour of chitosan crosslinking using glutaraldehyde (0.5 vol %) at 4 °C; Inset shows the determination of gelation point.

desired pressure for a set period of time. Subsequently it was depressurised using a gradient-depressurisation process and the resultant hydrogel was collected and immersed in 0.1 M Tris buffer solution for 1 h to inhibit further crosslinking and stored in PBS for characterisations.

The volume expansion of solution was monitored using a view cell (Jerguson sight gauge, series 13 No.32). The volume of the high pressure vessel was calibrated prior to measuring volume expansion of each solution [22].

2.4. Fabrication of microchannels in porous chitosan hydrogel

A custom-made needle array (500 μm diameter and 25 mm length) was placed on the top of chitosan solution in the high pressure vessel to create microchannels within the chitosan hydrogel. The custom made needle array was designed to ensure no obstacle was formed for the solution expansion during the hydrogel formation. After the process, the needle array was carefully removed from the vessel and the resultant hydrogel with microchannels was collected and post-treated as previously described.

2.5. In vitro cell culture

In vitro cell culturing was performed for different chitosan samples: porous hydrogels fabricated using1 wt % and 5 wt % AG (AG1 and AG5); the ones with small pores (LP) and non-porous chitosan hydrogels (NP) were produced in previous studies [11]. The hydrogels (∼8 mm diameter and 3 mm thickness) were transferred into a 48-well plate and washed with ethanol at least twice for sterilisation. Each hydrogel was then rinsed with culture media (DMEM, 10% FBS, 1% pen-strep) to remove the residual ethanol and immersed in this media at 37 °C overnight. The cells (human skin fibroblast cells GM3348) were then seeded (pipetted) onto the hydrogel at a concentration of 1×10^5 cells/sample. (For MTS assay, a cell concentration of 1×10^4 cells/sample was used). The cell-seeded hydrogels were kept in a CO$_2$ incubator (Thermo Fisher HERAcell 150i) at 37 °C for further characterisations. The media was refreshed every two days.

2.6. Characterisations

2.6.1. Scanning electron microscopy analysis

The surface morphologies of the resultant hydrogels were analysed using scanning electron microscopy (SEM Philip XL30). In this study, a cryo-SEM technique was used without any dehydration or coating treatment [11,23]. In brief, the fresh sample was mounted on a brass block. The block was then immersed in liquid nitrogen for 45 s, and immediately transferred into vacuum chamber ($<1.3 \times 10^{-4}$ mbar) for viewing at 15 kV. The snap freezing of the hydrogel ensured that the images acquired represented a snap shot of the actual hydrogel structure

[23]. Equivalent circle diameter (ECD) of the pores was calculated by using Image J software. At least 300 pores were analysed at each condition.

2.6.2. X-ray micro-computed (CT) tomography

The 3D structures of resultant hydrogels were investigated using Skyscan high-resolution desktop X-ray CT scanner (Skyscan, 1072, Belgium). X-ray tube current 100 μA and voltage 40 kV was used to obtain 3D reconstructed images. Each sample was mounted vertically on a plastic support and rotated 360° around the z-axis of the sample. 3D reconstruction of the sample was carried out using axial bitmap images and analysed by VG Studio Max software (Volume Graphics GmbH, Heidelberg, Germany). The overall porosity of each sample was obtained based on 3D reconstruction images (>150 images) using a built-in software (CT-An) [24].

2.6.3. Equilibrium swelling ratio (ESR)

The swelling behaviours of the porous hydrogels were evaluated at 37 °C, in PBS (pH 7.2–7.4). After immersion in excessive PBS at 37 °C overnight (at least 12 h), the swollen chitosan hydrogels were weighted (W_t). The hydrogels were subsequently lyophilised overnight, and the dry weights were recorded (W_0). The ESR was subsequently calculated as $(W_t-W_0)/W_0$.

2.6.4. Compressive properties

Uniaxial compression tests were performed in an unconfined state by using an Instron (Model 5543) with a 500 N load cell in the hydrated state (PBS) at 37 °C. Prior to mechanical testing, the hydrogels were immersed for at least 2 h in PBS; the thickness (∼3 mm) and diameter (∼8 mm) of each sample were measured using a digital calliper (J.B.S). The compression (mm) and load (N) were collected at a crosshead speed of 30 μm/s and 40% of final strain level. The compressive moduli were then calculated as the tangent slope of the stress-strain curves within linear regions.

2.6.5. Live/dead staining

Cell penetration and proliferation in the fabricated hydrogels were examined by live/dead staining. The cell-seeded hydrogels were sliced gently by a razor blade (Sterling) into ∼2 mm thick sections and stained with fluorescein diacetate (FDA) and propidium iodide (PI) (both 1 μg/ml in PBS) for 5 min. The stained samples were assessed using confocal laser scanning microscopy (CLSM, Nikon Limo). Live cells were stained fluorescent green due to intracellular esterase activity that de-acetylated FDA to a green florescent product. Dead cells were stained fluorescent red as their compromised membranes were permeable to nucleic acid stain (PI). Percent cell viability values were calculated by counting the number of live (green) cells and the number of dead (red) cells on CLSM images (10× magnification). The values were obtained by dividing the number of live cells by the number of total cells (live cells + dead cells). The values for AG1 and AG5 according to distance from the top surface were obtained in a similar manner; the data was binned into 3 vertical
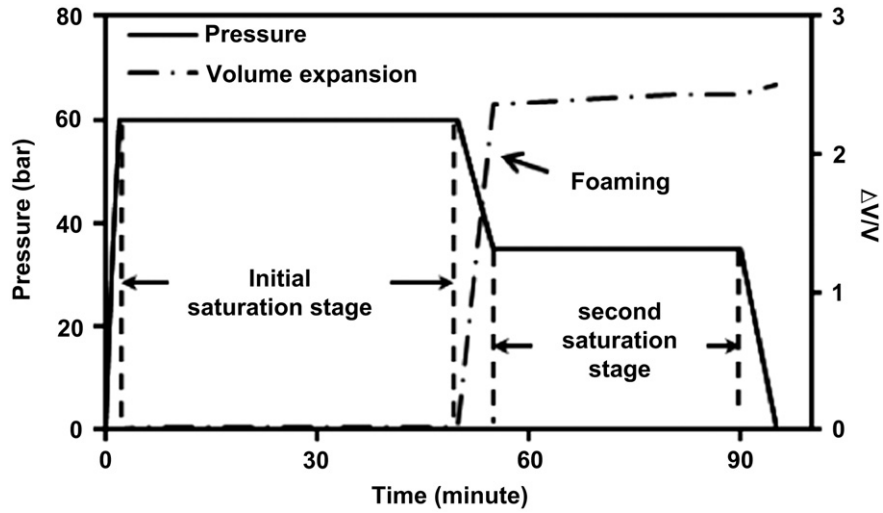
Fig. 3. Design of a gradient-depressurisation process and corresponding volume expansion rate.
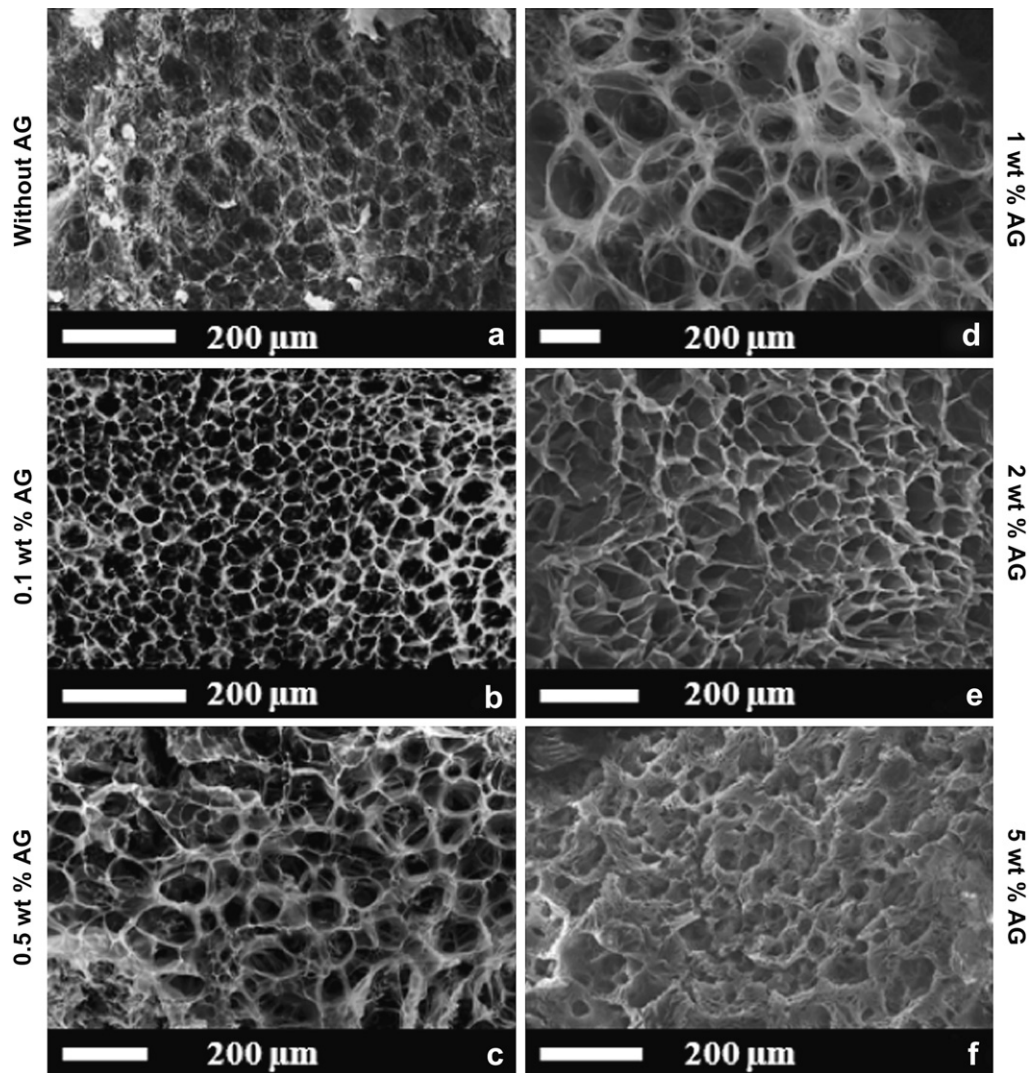
Fig. 4. SEM images of porous chitosan hydrogels with different initial AG weight ratios from (a) 0 wt % to (f) 5 wt %.
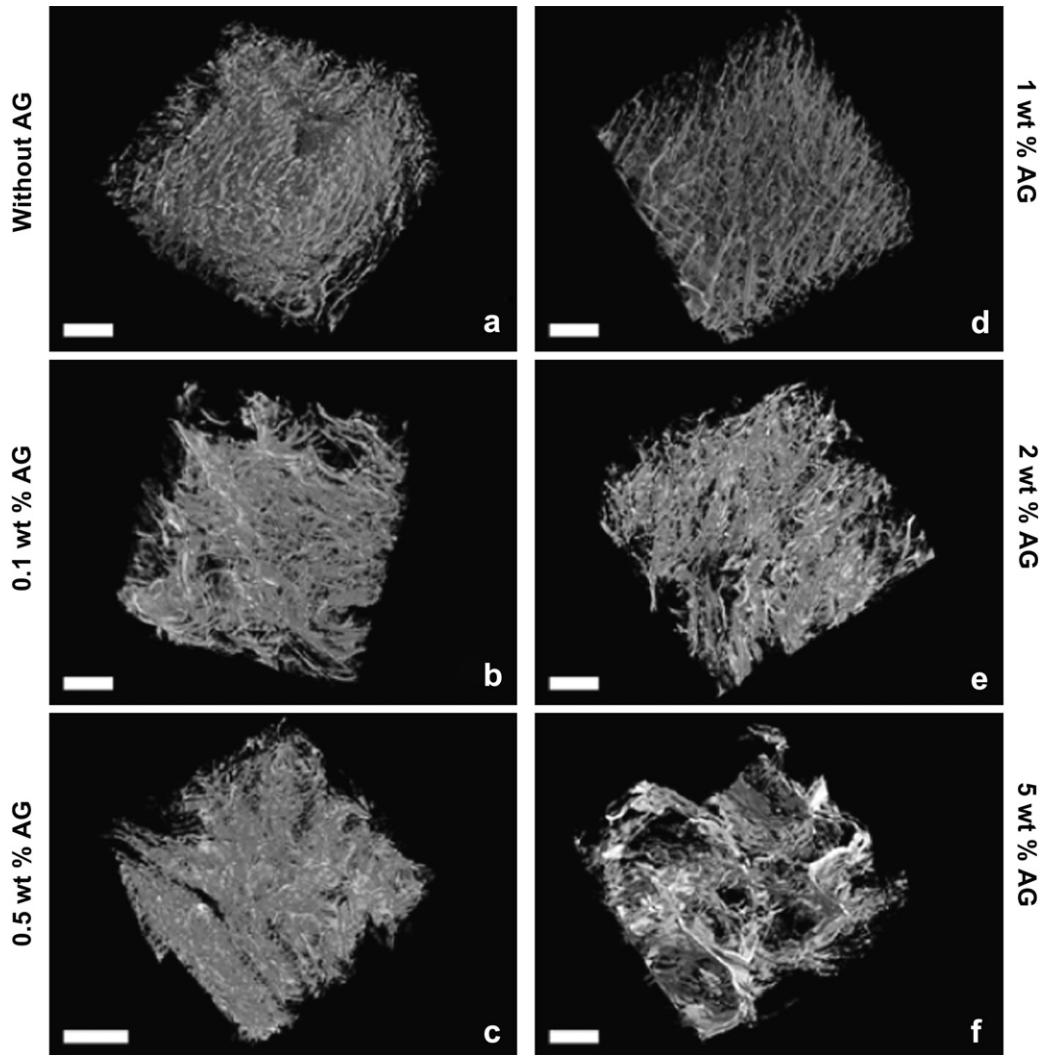
Fig. 5. Micro-CT images of porous chitosan hydrogels with different initial AG weight ratios from (a) 0 wt % to (f) 5 wt %; scale bars show 1 mm.

zones of 1000 μm × 200 μm each. A statistical significance level of 99.5% ($p < 0.005$) was considered to avoid potential human error in cell counting ($n = 9$).

2.6.6. In vitro proliferation assay

In vitro cell proliferation was examined by using MTS assay. The cell-seeded hydrogels (1×10^4 cells/sample) were immersed in culture medium within 48 well-plates ($n = 15$). At different time intervals (3 h, 1 day, 7 and 14 days), the samples were rinsed by PBS three times; 250 μL fresh medium and 50 μL MTS was subsequently added into each well. The samples were then kept in a CO_2 (5% CO_2 and 95% humidity) incubator at 37 °C for 1 h; allowing MTS to react with metabolically active cells and subsequently result in water-soluble formazan product quantifiable by the optical density (O.D.) at 490 nm by using a microplate reader (Bio Rad 680).

2.7. Statistical analysis

Each test was repeated three times. The statistical significance was determined at each condition (except elsewhere mentioned) by an independent Student's *t*-test for two groups of data using SPSS statistical software (PASW Statistics 18). Data are represented as mean ± standard deviation (SD). Confidence level of 95% ($p < 0.05$) was considered as statistically significant except elsewhere mentioned.

3. Results and discussions

3.1. Design of a gradient-depressurisation process to enhance porosity in chitosan

In a previous study we were able to create porosity in chitosan hydrogel using high pressure CO_2. Chitosan was dissolved in an aqueous phase that contained 0.5 vol % glutaraldehyde and the system was pressurised by CO_2 at 60 bar and 4 °C. After a period of 90 min the system was depressurised. In these hydrogels, the proportion of large pores (>80 μm) that are desirable for cell penetration was less than 2% [11]. We anticipated that the depressurisation stage, particularly prior to complete crosslinking of hydrogels can have a significant impact on the creation of
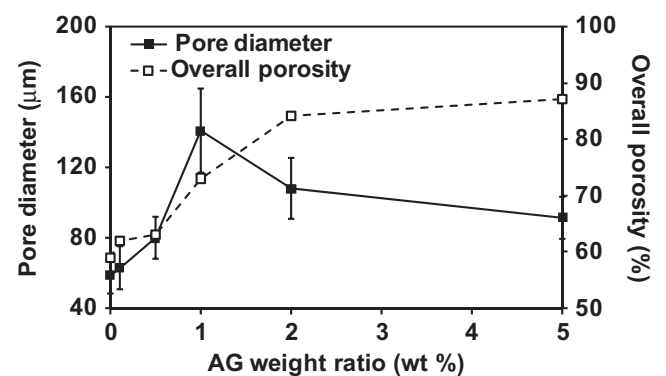
Fig. 6. Pore diameter and overall porosity of chitosan hydrogels with different initial AG weight ratios.

a polymer-lean phase (bubbles) and consequently porosity. The addition of surfactant can also increase the size of these bubbles by decreasing the interfacial tension between aqueous solution and CO_2 gas during depressurisation. A gradient-depressurisation profile was then developed to increase the pore size. The process involved a two-stage depressurisation profile. The initial depressurisation was commenced prior to complete crosslinking and the system was maintained at a certain pressure, which resulted in the creation of larger bubbles due to lower viscosity of the chitosan solution. The system was eventually depressurised to atmospheric pressure after crosslinking, and the resultant chitosan hydrogels were collected. The key parameters in this process were optimised. These parameters included an initial saturation pressure, the set point for the first stage depressurisation, final saturation pressure and total processing time.

Prior to performing the high pressure process, the rheological behaviour of chitosan crosslinked with GA was assessed at atmospheric pressure. As shown in Fig. 2, at 4 °C when using 0.5 vol % glutaraldehyde, the storage modulus (G′) of chitosan was increased over time dramatically due to crosslinking. The gelation point was 51.8 ± 0.4 min, indicating that chitosan solution behaved as a solid rather than liquid after this period (i.e. viscosity was increased dramatically). This result is consistent with our previous visual observation of chitosan crosslinking at the same conditions, underlining that at least 1 h was required to form partial-gelled chitosan [11]. The addition of AG within 0.1 wt %–5 wt % concentrations had no significant impact on the gelation point of chitosan solution. The solid-like behaviour impeded the volume expansion of chitosan system during depressurisation, which subsequently resulted in small pore size and limited porosity.

Our previous data demonstrated a volume expansion of less than 50% for the system that the hydrogels were formed by depressurisation after crosslinking (90 min) [11]. In this study, we depressurised the solution before gelation point (at 50 min) to achieve maximum volume expansion prior to complete crosslinking. The chitosan solution was expanded when the pressure of the system was decreased from initial saturation pressures (60–150 bar) to 35 bar due to the bubble formation and evaporation of CO_2 in aqueous solution at this pressure. Continuous depressurisation to atmospheric pressure at this stage resulted in a viscous liquid due to inadequate crosslinking. Therefore, the pressure was kept at 35 bar for a period of time, to induce volume expansion during chitosan crosslinking. Depressurisation during crosslinking significantly enhanced the volume expansion of chitosan system. The volume expansion was increased to over 150% when the system was depressurised and maintained at 35 bar after 50 min. The total processing time was kept at 90 min, which was adequate to produce a rigid chitosan hydrogel using glutaraldehyde at 4 °C [11]. Depressurisation at earlier than 50 min was not efficient in maintaining the bubbles in the aqueous phase. This effect may be due to the low viscosity of solution. The optimised gradient-depressurisation profile was illustrated in Fig. 3.

Visual observations show that resultant chitosan hydrogels were rigid and kept the original shape of the high pressure vessel, and the porous structure was depicted in Fig. 4(a) and Fig. 5(a). The pore size of the fabricated hydrogels using a gradient-depressurisation process was 59 ± 10 μm and the overall porosity was 59% (Fig. 6). The gradient-depressurisation process that was optimised resulted in a two-fold increase in pore size compared with the system that depressurisation was performed after crosslinking (32 μm in average) [11]. This enhancement was due to bubble formation and volume expansion of solution during the depressurisation at 35 bar and 50 min (before gelation point); these bubbles integrated and formed large size bubbles (CO_2 phase) in the solution, which led to the formation of large pores after complete crosslinking.
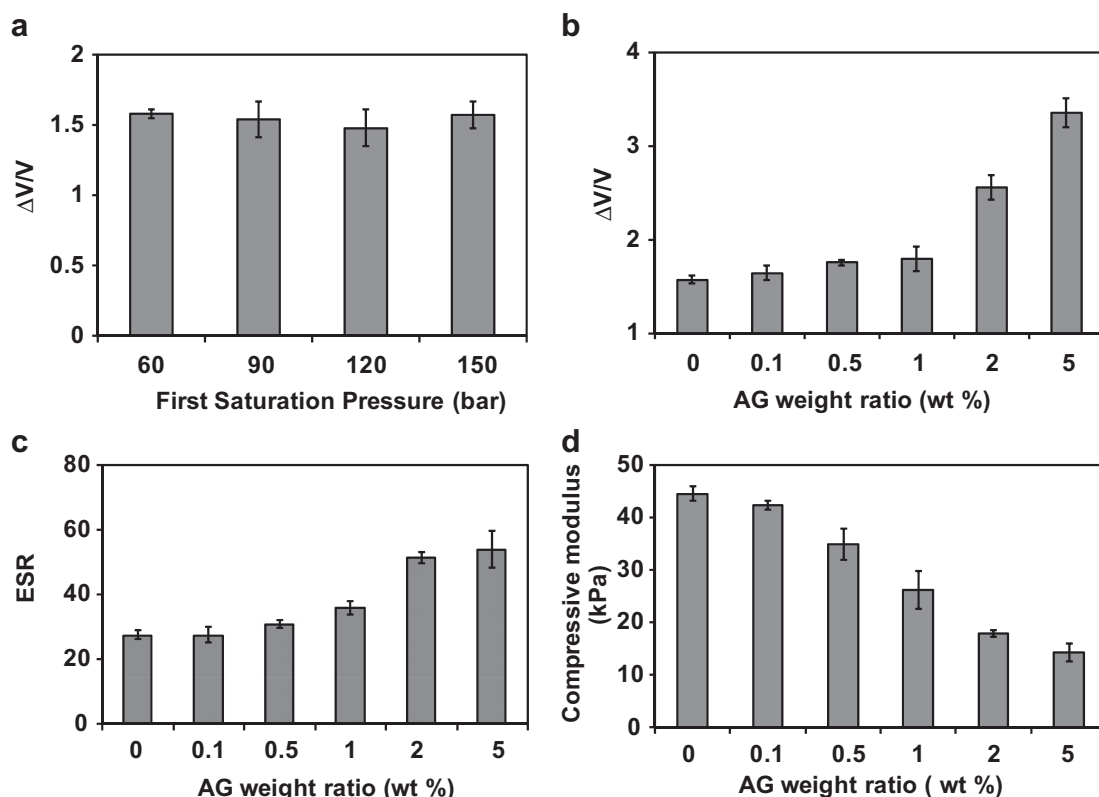
Fig. 7. Volume expansion ratio of chitosan solution at (a) different initial saturation pressures and (b) with different initial AG weight ratios; (c) ESR and (d) compressive modulus of chitosan hydrogels with different initial AG weight ratios.

As depicted in Fig. 7(a), increasing the initial pressure of the high pressure process from 60 bar to 150 bar had a negligible effect on the volume expansion of solution at the stage of depressurisation. This effect was attributed to the negligible increase in CO_2 solubility in the aqueous system within the pressure range examined [11,25]. Therefore, the initial saturation pressure of 60 bar was used for the rest of study.

3.2. The effect of surfactant on porosity generation in chitosan

A preliminary test was conducted to assess the feasibility of creating porosity in chitosan using CO_2 gas flow (∼10 bar) as a foaming agent. Chitosan was dissolved in solution containing 5 wt % AG and 0.5 vol % glutaraldehyde and CO_2 was added via a frit to this solution for a period of 90 min. The average pore diameter produced was 150 μm and the porosity was below 30%. These results indicate that the addition of AG has negligible effect on CO_2 absorption in chitosan, and a CO_2 saturation stage (under high pressure) is essential to produce interconnected pores in chitosan.

The addition of AG on the pore characteristics of chitosan hydrogels fabricated by the gradient-depressurisation process was investigated. Chitosan solution contained 0.1–5 wt % AG was maintained transparent upon pressurisation up to 60 bar, underlining that no phase separation occurred and both chitosan and AG were soluble in aqueous system at the conditions examined. Our results show that the increasing AG weight ratio in chitosan led to higher volume expansion. As shown in Fig. 7(b), the volume

expansion (ΔV/V) was increased slightly from 157% to 179% when AG weight ratio was raised from 0 to 1 wt %. A remarkable volume expansion of 256% and 336% was observed when chitosan solution containing 2 wt % and 5 wt % AG was used, respectively. These results indicate that the addition of 2 wt % and 5 wt % AG significantly decreased the interfacial tension between CO_2 and chitosan solution during depressurisation.

The addition of AG in the chitosan solution had a beneficial impact on the desired pore size and overall porosity (Figs. 4 and 5). As shown in Fig. 6, the average pore diameter of resultant hydrogels ranged from 63 μm to 140 μm. The pore diameters were a function of the initial AG weight ratio in chitosan. Increasing the initial AG weight ratio resulted in enhanced pore diameter. As the AG weight ratio was increased from 0.1 to 1 wt %; the pore diameter was enhanced from 63.1 ± 12 μm to 140.6 ± 24 μm. This enhancement was attributed to the foaming effect of AG, which decreased the interfacial tension of system (between CO_2 and chitosan during depressurisation) compared with that of pure chitosan solution. Upon depressurisation, lower interfacial tension allowed for larger pore formation [8,26]. The use of higher AG weight ratio (ie. 2 wt % and 5 wt %) in chitosan did not enhance the pore size. The average pore diameter was 107.9 ± 17 μm and 91.6 ± 12 μm, respectively. The significant decrease in average pore diameter may be attributed to the formation of higher number of gas bubble nuclei during the depressurisation stage, which resulted in smaller pores [27–31].

The optimal pore diameter for the regeneration of adult mammalian skin, osteoid ingrowth, and bone regeneration are
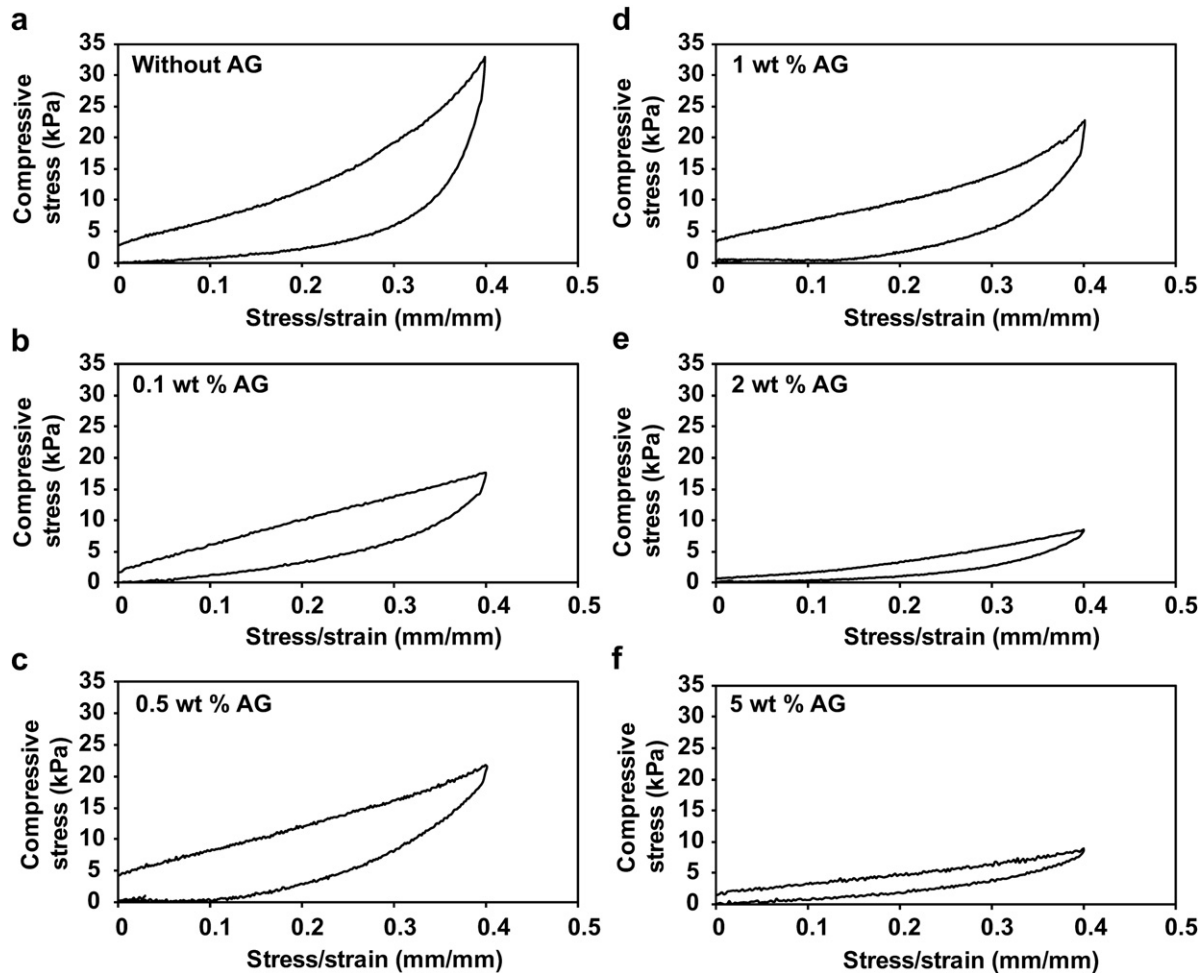
Fig. 8. Compressive stress/strain curves of fabricated hydrogels with different initial AG weight ratios from (a) 0 wt % to (f) 5 wt %.
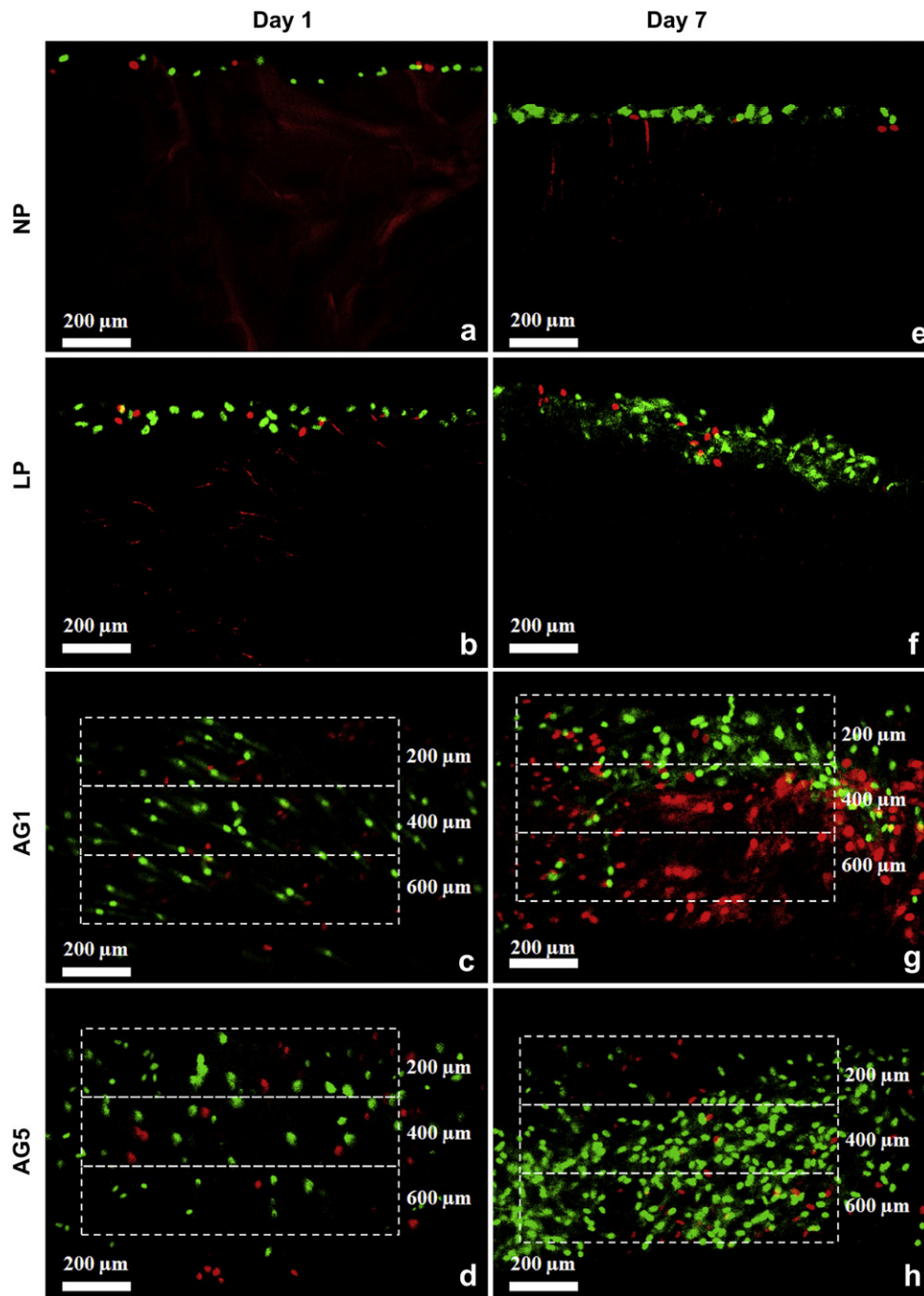
Fig. 9. CLSM images of cell-seeded chitosan hydrogels on cross section. (a and e) NP: non-porous chitosan hydrogels produced at atmospheric condition; (b and f) LP: porous chitosan produced as described in previous studies [11] with small pore size of 32 μm in average; (c, d, g and h) AG1 and AG5: chitosan hydrogels produced using a gradient-depressurisation process with (c and g) 1 wt % AG, and (d and h) 5 wt % AG, respectively (same codes are used below). Left panel shows the images on day 1 and right on day 7.

20–125 μm [32]; 40–100 μm and 100–350 μm [33], respectively. The process developed in this study allows greater control over the pore size of chitosan hydrogel by varying the depressurisation profile and surfactant concentration. Therefore, the porosity of hydrogels can be more finely tuned to a desired level for different tissue engineering applications [34,35].

The overall porosity of resultant hydrogels was increased monotonically from 59% to 87% when the concentration of AG was elevated from 0 wt % to 5 wt % (Fig. 6). Increasing AG weight ratio enhanced the degree of foaming and the volume expansion of aqueous solution leading to creation of higher porosity. The effect

of pore characteristics acquired on the swelling, mechanical and biological properties of the hydrogels were investigated.

3.3. Equilibrium swelling ratio (ESR)

The swelling plays a significant role in regulating nutrients and wastes exchange in hydrogel. In this study, porous chitosan hydrogels exhibited ESR from 27.4 ± 1 to 53.9 ± 6 as AG weight ratio was increased from 0 wt % to 5 wt % as depicted in Fig. 7(c). As expected, higher AG weight ratio in the system caused higher porosity, which provided larger contact surface area between the hydrogel and
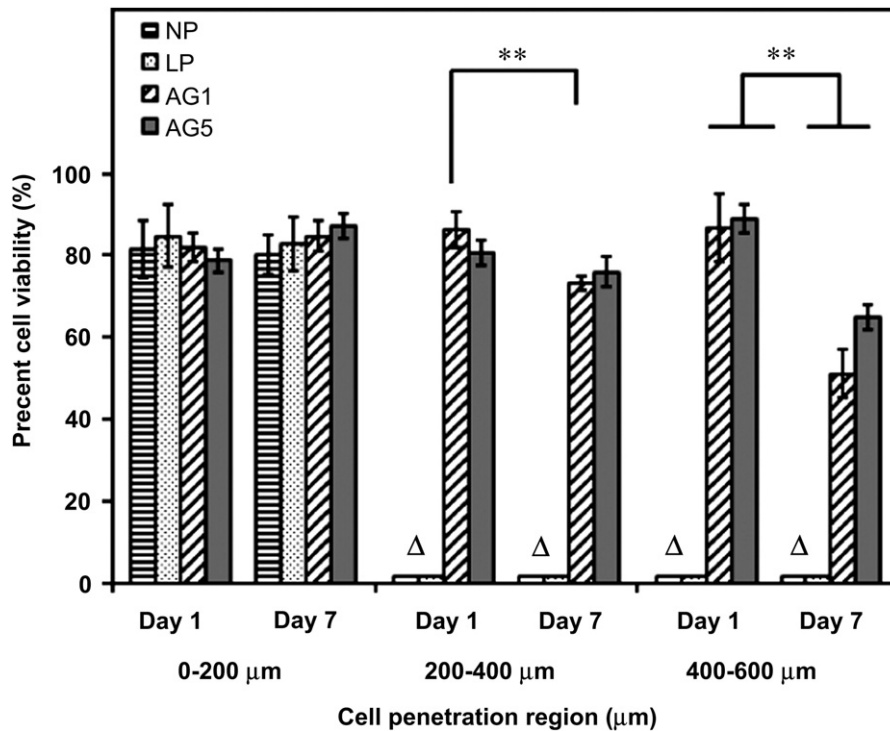
Fig. 10. Precent cell viability in chitosan hydrogels produced at different conditions at different times post-seeding ($n = 9$). Student's t-tests were performed to demonstrate difference between two groups (**$p < 0.005$). Δ: data not determined due to absence of cells at these regions.

media, and resulted in higher ESR. These results were in agreement with previous studies that porous glutaraldehyde-crosslinked chitosan hydrogels exhibited more than two fold higher ESR than non-porous equivalents [9,11,36–38]. Wu et al. also demonstrated the swelling ratio of freeze-dried collagen/chitosan scaffolds was increased from 20 to 44 due to the enhancement of contact surface area [36]. The resultant chitosan hydrogels show high potential due to its similar swelling properties compared with other hydrogels for various tissue engineering applications [39–43].

3.4. Mechanical characterisations

Adequate mechanical strength is required for hydrogels in tissue engineering. The compressive stress-strain curves of the fabricated hydrogels were shown in Fig. 8. Most of the samples exhibited linear stress-strain curves with up to 40% strain rate. The compressive moduli were thus calculated within linear regions. As shown in Fig. 7(d), pure chitosan porous hydrogels exhibited a compressive modulus of 44.6 ± 1 kPa. No significant difference was found when a 0.1 wt % AG weight ratio was used (42.4 ± 1 kPa). However, the compressive modulus was decreased significantly from 34.8 ± 3 kPa to 14.3 ± 2 kPa, as the AG weight ratio was increased from 0.5 wt % to 5 wt % (Fig. 7(d)). These results can be explained by the enhanced porosity due to the increase of AG weight ratio. Previous studies also demonstrate the negative impact of porosity on compressive modulus [11,44–46]. Glutaraldehyde-crosslinked porous chitosan hydrogels possessed a compressive modulus of 41.6 kPa, and the non-porous equivalents exhibited a compressive modulus of 135.1 kPa, due to the absence of porosity [11]. Lin et al. demonstrated that the compressive moduli of porous poly (L-lactide-co-D,L-lactide) scaffolds were decreased from 168 to 44 MPa as the porosity increased from 58% to 80% [46]. The correlation between porosity and compressive modulus confirm that the mechanical properties of resultant porous chitosan hydrogels are tunable by controlling the

porosity. The compressive moduli of fabricated porous chitosan hydrogels are within the range of various natural tissues, such as human contracted smooth muscle (10 kPa), and human thyroid ($\sim$10 kPa) [47–49]. The resultant hydrogels can be used for the preparation of organs that require low mechanical strength before the cell growth or for the in vitro tissue engineering applications with low pressure load.

3.5. In vitro cell culture

In vitro cell culture studies were conducted to demonstrate the effect of enhanced pore size and porosity in chitosan hydrogel on
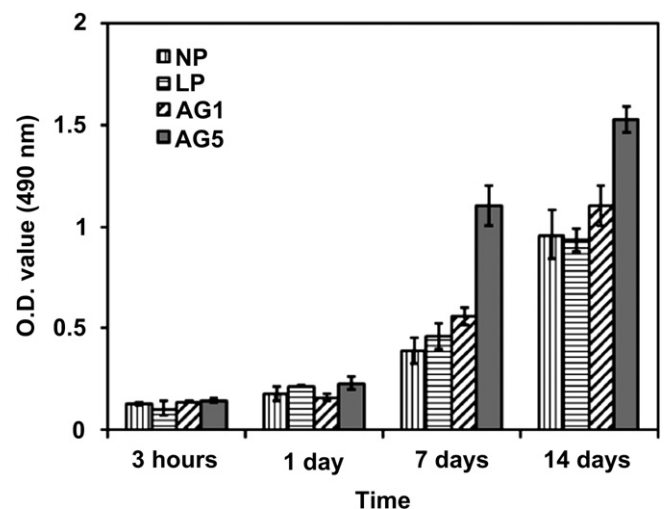
Fig. 11. MTS analysis on chitosan hydrogels produced at different conditions at different times post-seeding ($n = 15$).
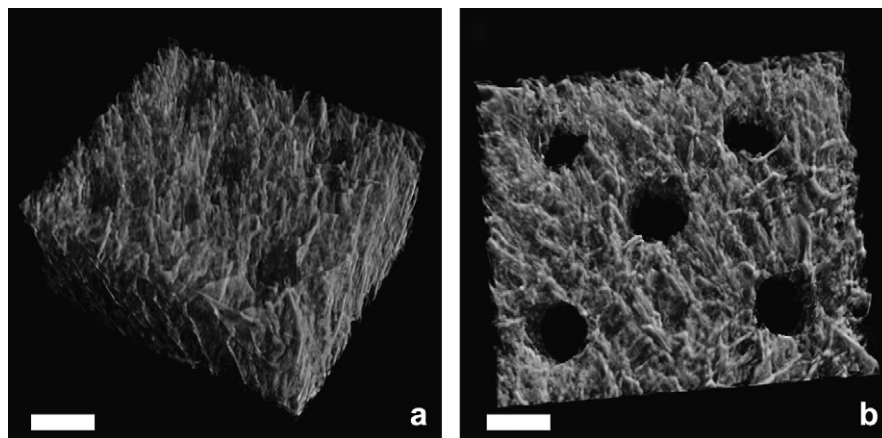
Fig. 12. Micro-CT images of a chitosan porous hydrogel with 5 wt % initial AG weight ratio with microchannels; (a) shows a panoramatic view and (b) a bird's-eye view; scale bars show 500 μm.

cell penetration and proliferation. Classic static cell seeding onto 3D scaffold relies on large pore size, allowing for cell penetration throughout the 3D structure and high overall porosity, facilitating nutrients and wastes exchange for cell proliferation [50]. Fibroblast cells were only able to adhere on the top surface of non-porous chitosan hydrogels (NP) (Fig. 9(a and e)). The presence of pores allowed cells to penetrate into porous hydrogels. However, the penetration distance was only 50–100 μm from top surface due to the small pore size (32 μm in average) in chitosan hydrogels (LP) that were previously produced (Fig. 9(b and f)) [11]. Increasing pore size had a beneficial effect on cell penetration depth. As shown in Fig. 9(c–d and g–h), fibroblast cells were uniformly distributed in a region of 600 μm from top surface within porous chitosan with 1 wt % and 5 wt % initial AG weight ratio (average pore diameter of 140 μm and 92 μm, respectively) with reasonable cell viabilities (~80%). Negligible numbers of cells were found in further regions from top surface (i.e. >600 μm). For this reason we primarily studied cell viabilities within 600 μm region from the top surface (i.e. 0–200 μm, 200–400 μm and 400–600 μm). Cells exhibited similar viabilities in the region of 0–200 μm from top surface in all the samples on day 1 upon seeding (Fig. 10). No significant drop in cell viability was found in this region on day 7. However, cells lost viabilities over time due to limited nutrients and wastes exchange in the deeper region. In particular, in the region of 200–400 μm, the cell viability in AG1 (porosity of 73%) was decreased to 73.0 ± 2% on day 7 compared with viability on day 1 (85.7 ± 4%). There was no significant difference in viability between day 1 and day 7 in AG5

(porosity of 87%). These results may be attributed to the increased porosity that resulted in enhanced mass transfer properties. In addition, in the region of 400–600 μm, both samples (i.e. AG1 and AG5) showed lower cell viabilities on day 7 (51.2 ± 7% and 64.4 ± 3%, respectively) in comparison to day 1 (85.0 ± 7% and 88.6 ± 4%, respectively). The data indicates that the enhanced pore size and porosity improved cell penetration. The optimised porous chitosan hydrogels with average pore diameter of 92 μm and overall porosity of 87% (AG5) could support cell penetration up to a 400 μm distance from top surface with reasonable cell viability (~80%).

MTS data further demonstrates the cell proliferation rate during *in vitro* culture within a period of 14 days. As shown in Fig. 11, the O.D. values were increased dramatically at day 7 and 14 for all the samples, corroborating cell proliferation. The overall cell proliferation rate was a function of porosity in hydrogels. AG5 exhibited remarkably higher proliferation rate than the others at day 7 and 14. This can be explained by the increased overall porosity within hydrogel which provided enhanced nutrients and wastes exchange.

3.6. The effect of microchannel

In this study, we further produced porous chitosan hydrogels (AG5) with aligned microchannels (500 μm diameter) as shown in Fig. 12, using a micromolding technique. MTS data indicates that the cell proliferation rate of chitosan hydrogels with aligned microchannels was similar to those without microchannels on day 7. However, as shown in Fig. 13, the results on day 14 demonstrate a significant increase in O.D. for the samples contained microchannels compared with those without such structure. These results may be attributed to the formation of fibroblasts confluent monolayer on the top surface of porous chitosan due to proliferation; this layer may impede nutrients and oxygen transfer to the deeper layer. Nonetheless, for samples with microchannels, the top layer was not completely covered with cells due to the large size of the microchannels, which facilitate nutrients and oxygen transfer for longer periods of time.

4. Conclusions

A rapid process was developed for the creation of porosity in chitosan hydrogel that involves dissolving high pressure CO_2 into an aqueous solution and using CO_2 gas as a foaming agent. The results demonstrate that the depressurisation profile had a significant impact on the pore characteristics of chitosan hydrogels. The addition of a non-toxic surfactant such as *A. gum* (AG) substantially
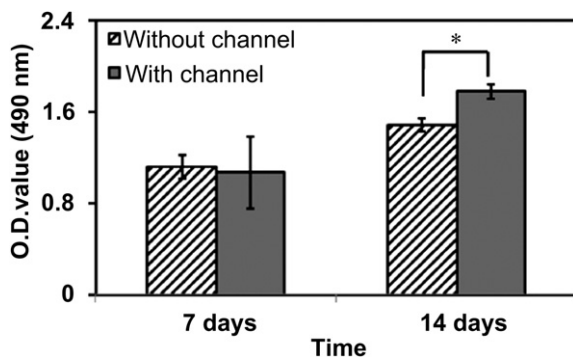
Fig. 13. MTS analysis on porous chitosan hydrogels without and with microchannels ($n = 15$) different times post-seeding. Student's *t*-tests were performed to demonstrate difference between two groups (*$p < 0.05$).

increased the pore size and porosity. Process variables can be controlled to generate chitosan hydrogels with a maximum average pore diameter of 140 μm and porosity of 87%, respectively. This new process eliminates the use of toxic solvent for pore formation in hydrogels. The presence of porosity improved the swelling ratio of chitosan hydrogels and subsequently enhanced cell proliferation rate. The cell proliferation rate was further improved by the fabrication of aligned microchannels within porous hydrogels that enhanced nutrients and wastes exchange. The fabricated chitosan hydrogels with controllable pore size and porosity have high potential for tissue engineering applications.

Acknowledgements

References

[1] Annabi N, Nichol JW, Zhong X, Ji C, Koshy S, Khademhosseini A, et al. Controlling the porosity and microarchitecture of hydrogels for tissue engineering. Tissue Eng Part B Rev 2010;16(4):371–83.

[2] Peppas NA, Hilt JZ, Khademhosseini A, Langer R. Hydrogel in biology and medicine: from molecular principles to bionanotechnology. Adv Mater 2006; 18:1345–60.

[3] Khademhosseini A, Langer R. Microengineered hydrogels for tissue engineering. Biomaterials 2007;28(34):5087–92.

[4] Khademhosseini A, Langer R, Borenstein J, Vacanti JP. Microscale technologies for tissue engineering and biology. Proc Natl Acad Sci U S A 2006;103:2480–7.

[5] Gerecht S, Townsend SA, Pressler H, Zhu H, Nijst CLE, Bruggeman JP, et al. A porous photocurable elastomer for cell encapsulation. Biomaterials 2007; 28:4826.

[6] Thomson RC, Wake MC, Yaszemski MJ, Mikos AG. Biodegradable polymer scaffolds to regenerate organs. In: Peppas N, Langer R, editors. Advances in polymer science. Berlin Heidelberg: Springer-Verlag; 1995. p. 245–74.

[7] Lee JY, Tan B, Cooper AI. CO_2-in-water emulsion-templated poly(vinyl alcohol) hydrogels using poly(vinyl acetate)-based surfactants. Macromolecules 2007; 40(6):1955–61.

[8] Palocci C, Barbetta A, La Grotta A, Dentini M. Porous biomaterials obtained using supercritical CO_2-water emulsions. Langmuir 2007;23(15):8243–51.

[9] Annabi N, Mithieux SM, Boughton EA, Ruys AJ, Weiss AS, Dehghani F. Synthesis of highly porous crosslinked elastin hydrogels and their interaction with fibroblasts in vitro. Biomaterials 2009;30(1):4550–7.

[10] Annabi N, Mithieux SM, Weiss AS, Dehghani F. The fabrication of elastin-based hydrogels using high pressure CO_2. Biomaterials 2009;30(1):1–8.

[11] Ji C, Annabi N, Khademhosseini A, Dehghani F. Fabrication of porous chitosan scaffolds for soft tissue engineering using dense gas CO_2. Acta Biomater 2011; 7(4):1653–64.

[12] Ji C, Barrett A, Poole-Warren Laura A, Foster NR, Dehghani F. The development of a dense gas solvent exchange process for the impregnation of pharmaceuticals into porous chitosan. Int J Pharm 2010;391:187–96.

[13] Barbetta A, Rizzitelli G, Bedini R, Pecci R, Dentini M. Porous gelatin hydrogels by gas-in-liquid foam templating. Soft Matter 2010;6:1785–92.

[14] Ling Y, Rubin J, Deng Y, Huang C, Demirci U, Karp JM, et al. A cell-laden microfluidic hydrogel. Lab Chip 2007;7:756.

[15] Brigham MD, Bick A, Lo E, Bendali A, Burdick JA, Khademhosseini A. Mechanical robust and bioadhesive collagen and photocrosslinkable hyaluronic acid semi-interpenetrating networks. Tissue Eng Part A 2008;15:1645.

[16] Song YS, Lin RL, Montesano G, Durmus NG, Lee G, Yoo SS, et al. Engineered 3D tissue models for cell-laden microfludic channels. Anal Bioanal Chem 2009; 395:185–93.

[17] Park JH, Chung BG, Lee WG, Kim J, Brigham MD, Shim J, et al. Microporous cell-laden hydrogels for engineered tissue constructs. Biotechnol Bioeng 2010;106:138.

[18] Di Martino A, Sittinger M, Risbud MV. Chitosan: a versatile biopolymer for orthopaedic tissue-engineering. Biomaterials 2005;26(30):5983–90.

[19] CFR. Code of federal regulations title 21 part 184; 2010.

[20] Winter HH, Chambon F. Analysis of linear viscoelasticity of a crosslinking polymer at the gel point. J Rheol (N Y N Y) 1986;30:367–82.

[21] Chambon F, Winter HH. Linear viscoelasticity at the gel point of a crosslinking PDMS with imbalanced stoichiometry. J Rheol (N Y N Y) 1987;31:683–97.

[22] Thiering R, Dehghani F, Dillow AK, Foster NR. The influence of operating conditions on the dense gas precipitation of model proteins. J Chem Technol Biotechnol 2000;75:29–41.

[23] Romeo TA. simple cold-block procedure for the SEM. Aust Electron Microsc Newsl 1996;52:16–8.

[24] Barbetta A, Gumiero A, Pecci R, Bedini R, Dentini M. Gas-in-liquid foam templating as a method for the production of highly porous scaffolds. Biomacromolecules 2009;10:3188–92.

[25] Dodds WS, Stutzman LF, Sollami BJ. Carbon dioxide solubility in water. Ind Eng Chem 1956;1:92.

[26] Rotuteau E, Marie E, Dellacherie E, Durand A. From polymeric surfactants to colloidal systems (3): neutral and anionic polymeric surfactants derived from dextran. Colloids Surf A Physicochem Eng Asp 2007;301:229–38.

[27] Goel SK, Beckman EJ. Generation of microcellular polymeric foams using supercritical carbon dioxide. II: cell growth and skin formation. Polym Eng Sci 1994;34(14):1148–56.

[28] Goel SK, Beckman EJ. Generation of microcellular polymeric foams using supercritical carbon dioxide. I: effect of pressure and temperature on nucleation. Polym Eng Sci 1994;34(14):1137–47.

[29] Tai H, Mather ML, Howard D, Wang W, White LJ, Crowe JA, et al. Control of pore size and structure of tissue engineering scaffolds produced by supercritical fluid processing. Eur Cell Mater 2007;14:64–77.

[30] Arora KA, Lesser AJ, McCarthy TJ. Preparation and characterization of microcellular polystyrene foams processed in supercritical carbon dioxide. Macromolecules 1998;31(14):4614–20.

[31] Nalawade SP, Westerman D, Leeke G, Santos RCD, Grijpma DW, Feijen J. Preparation of porous poly(trimethylene carbonate) structures for controlled release applications using high pressure CO_2. J Control Release 2008;132(3): e73–5.

[32] Yannas IV, Lee E, Orgill DP, Skrabut EM, Murphy GF. Synthesis and characterization of a model extracellular matrix that induces partial regeneration of adult mammalian skin. Proc Natl Acad Sci U S A 1989;86(3):933–7.

[33] Whang K, Healy KE, Elenz DR, Nam EK, Tsai DC, Thomas CH, et al. Engineering bone regeneration with bioabsorbable scaffolds with novel microarchitecture. Tissue Eng 1999;5:35.

[34] Heyde M, Partridge K, Howdle SM, Oreffo ROC, Garnett M, Shakesheff KM. Development of a slow non-viral DNA release system from $P_{DL}LA$ scaffolds fabricated using a supercritical CO_2 technique. Biotechnol Bioeng 2007;98: 679–93.

[35] Kanczler JM, Ginty PJ, White L, Clarke N, Howdle SM, Shakesheff KM, et al. The effect of the delivery of vascular endothelial growth factor and bone morphogenic protein-2 to osteoprogenitor cell populations on bone formation. Biomaterials 2010;31:1242–50.

[36] Wu X, Black L, Santacana-Laffitte G, Patrick Jr CW. Preparation and assessment of glutaraldehyde-crosslinked collagen-chitosan hydrogels for adipose tissue engineering. J Biomed Mater Res A 2007;81(1):59–65.

[37] Wojtasz-Pajak A, Brzeski MM, Malesa-Ciecwierz M. Regulatory aspects of chitosan and its practical applications. In: Karnicki Z, Wojtasz-Pajak A, Brzeski M, Bykowski P, editors. Chitin world. Bremerhaven: Wirtschaftsverlag NW; 1994. p. 435–45.

[38] Lin Y, Tan F, Marra KG, Jan S, Liu D. Synthesis and characterization of collagen/hyaluronan/chitosan composite sponges for potential biomedical applications. Acta Biomater 2009;5:2591.

[39] Ma L, Gao C, Mao Z, Zhou J, Shen J, Hu X, et al. Collagen/chitosan porous scaffolds with improved biostability for skin tissue engineering. Biomaterials 2003;24(26):4833–41.

[40] Chen KY, Liao WJ, Kou SM, Tsai FJ, Chen YS, Huang CY, et al. Asymmetric chitosan membrane containing collagen I Nanospheres for skin tissue engineering. Biomacromolecules 2009;10:1642–9.

[41] Kathuria N, Tripathi A, Kar KK, Kumar A. Synthesis and characterization of elastic and macroporous chitosan-gelatin cryogels for tissue engineering. Acta Biomater 2009;5:406–18.

[42] Silva SS, Motta A, Rodrigues MT, Pinheiro AFM, Gomes ME, Mano JF, et al. Genipin-cross-linked chitosan silk fibroin sponges for cartilage engineering strategies. Biomacromolecules 2008;9:2764–74.

[43] Tan H, Chu Constance R, Payne KA, Marra Kacey G. Injectable in situ forming biodegradable chitosan-hyaluronic acid based hydrogels for cartilage tissue engineering. Biomaterials 2009;30:2499–506.

[44] Soliman S, Sant S, Nichol JW, Khabiry M, Traversa E, Khademhosseini A. Controlling the porosity of fibrous scaffolds by modulating the fiber diameter and packing density. J Biomed Mater Res A 2011;96:566–74.

[45] Karageorgiou V, Kaplan D. Porosity of 3D biomaterial scaffolds and osteogenesis. Biomaterials 2005;26(27):5474–91.

[46] Lin A, Barrow T, Cartmell S, Guldberg RE. Microarchitectural and mechanical characterization of oriented porous polymer scaffolds. Biomaterials 2003; 24(3):481–9.

[47] Amsden B. Curable, biodegradable elastomers: emerging biomaterials for drug delivery and tissue engineering. Soft Matter 2007;3:1335–48.

[48] Levental I, Georges P, Janmey P. Soft biological materials and their impact on cell function. Soft Matter 2007;3(3):299–306.

[49] Shin H, Nichol JW, Khademhosseini A. Cell-adhesive and mechanically tunable glucose-based biodegradable hydrogels. Acta Biomater 2011;7:106–14.

[50] Buckley CT, O'Kelly KU. Maintaining cell depth viability: on the efficacy of a trimodal scaffold pore architecture and dynamic rotational culturing. J Mater Sci Mater Med 2010;21:1731–8.